Taylor & Francis
Taylor & Francis Group

International Journal of Digital Earth

ISSN: (Print) (Online) Journal homepage: www.tandfonline.com/journals/tjde20

A graph autoencoder network to measure the geometric similarity of drainage networks in scaling transformation

Huafei Yu, Tinghua Ai, Min Yang, Weiming Huang & Lars Harrie

INTERNATIONAL JOURNAL OF DIGITAL EARTH
2023, VOL. 16, NO. 1, 1828–1852
https://doi.org/10.1080/17538947.2023.2212920

A graph autoencoder network to measure the geometric similarity of drainage networks in scaling transformation

Huafei Yu [a,b], Tinghua Ai [a], Min Yang [a], Weiming Huang [c] and Lars Harrie [b]

[a]School of Resource and Environmental Sciences, Wuhan University, Wuhan, People's Republic of China; [b]Department of Physical Geography and Ecosystem Science, Lund University, Lund, Sweden; [c]School of Computer Science and Engineering, Nanyang Technological University, Singapore, Singapore

ABSTRACT
Similarity measurement has been a prevailing research topic in geographic information science. Geometric similarity measurement in scaling transformation (GSM_ST) is critical to ensure spatial data quality while balancing detailed information with distinctive features. However, GSM_ST is an uncertain problem due to subjective spatial cognition, global and local concerns, and geometric complexity. Traditional rule-based methods considering multiple consistent conditions require subjective adjustments to characteristics and weights, leading to poor robustness in addressing GSM_ST. This study proposes an unsupervised representation learning framework for automated GSM_ST, using a Graph Autoencoder Network (GAE) and drainage networks as an example. The framework involves constructing a drainage graph, designing the GAE architecture for GSM_ST, and using Cosine similarity to measure similarity based on the GAE-derived drainage embeddings in different scales. We perform extensive experiments and compare methods across 71 drainage networks during five scaling transformations. The results show that the proposed GAE method outperforms other methods with a satisfaction ratio of around 88% and has strong robustness. Moreover, our proposed method also can be applied to other scenarios, such as measuring similarity between geographical entities at different times and data from different datasets.

ARTICLE HISTORY
Received 1 March 2023
Accepted 7 May 2023

KEYWORDS
Geometric similarity measurement; drainage network; scaling transformation; graph autoencoder network

1. Introduction

Similarity measurement is a common technique in geographic information science for comparing the likeness between two or more geographic objects. It is primarily used in three scenarios: comparing geographical entities at different times, comparing data from different datasets, and comparing geographical features at various scales. Among these scenarios, similarity measurement in scaling transformation is widely used to quantify the proportion of spatial information in the transmission process (Ai et al. 2014; Yan, Shen, and Li 2016) and to guide the multi-scale expression of geographical features (Yan 2019; Liu et al. 2022; Yan 2022). It includes both semantic and geometric similarity measurement, with the latter being the focus of this study. However, *geometric similarity measurement in scaling transformation* (GSM_ST) has always been an uncertain issue of geographic information science.

The uncertainty in GSM_ST can be divided into three categories: (1) GSM_ST involves subjective judgments that depend on spatial cognition (Gao and Cao 2021). Different individuals may

CONTACT Tinghua Ai tinghuaai@whu.edu.cn

have varying opinions on what constitutes a high level of similarity, resulting in a variance of GSM_ST. (2) GSM_ST has different concerns, such as a comparison at a global scale that may overlook important local details. Different map generalization operators may preserve different aspects of the original map, such as selection focusing on the global structure (Zhang and Guilbert 2017) and simplification focusing on the local detail (Ai et al. 2017), leading to varying targets of GSM_ST. (3) The parameters used for GSM_ST are diverse and complex. GSM_ST is a multidisciplinary problem involving mathematical geometry, cartography, and cognition. Numerous parameters, such as direction, bending, density, and classification, can be used to express geometric and topological features. However, choosing one or several as the typical features for GSM_ST is challenging. The rule-based methods are usually used to address these uncertainties in GSM_ST through a weighted calculation based on the similarity of different relations, such as direction, distance, and topology (Yan, Shen, and Li 2016). The similarity in each relation is the ratio of several representative parameters before and after the scaling transformation (Yan and Li 2015; Yang and Wang 2021). However, the rule-based approach requires adjusting parameters and weights for different objects, leading to poor robustness in addressing the uncertainty of GSM_ST, for example, adjusting parameters such as road density and length for road networks, river ordering and flow direction for river networks, and building area and direction. Likewise, the vector-based method, supported by techniques such as the Fourier transform, is limited by the fixed length of the shape descriptor and cannot be applied to a group object such as road networks or drainage networks (Liu et al. 2022). Therefore, due to its uncertainty, the GSM_ST remains a challenge.

In general, the GSM_ST methods mentioned above aim to calculate the difference in spatial cognition information. The rule-based method uses local spatial relations, such as topology, distance, and direction, while the vector-based method uses global morphological vectors. This process can be formally expressed as $f(\boldsymbol{x}, \boldsymbol{x}')$ where $\boldsymbol{x} \in \mathbb{R}^{1\times n}$ and $\boldsymbol{x}' \in \mathbb{R}^{1\times n}$ are the vectors of spatial cognition information before and after scaling transformation, respectively, and $f(\cdot)$ denotes a function calculating the vector difference, usually using Cosine similarity (Zhang and Yu 2022). Thus, it is important for GSM_ST to mine deep-level information or a representation that captures the spatial cognition information with great uncertainty. However, due to the uncertainty of GSM_ST, choosing one or more features to map the spatial cognition information directly is difficult, resulting in a lack of robustness and self-learning ability. Therefore, further research on how to derive accurate spatial cognition information based on limited morphological knowledge remains crucial.

Deep learning is a powerful tool for uncovering implicit information from raw data, like RGB values of remote sensing images or coordinates of trajectory data, and basic features such as direction, length, area, and angle of vector elements. It has successfully solved many uncertain geospatial cognition problems (Yan et al. 2021; Li, Yan, and Lu 2022; Yu et al. 2022) by encoding the raw data into the features at different levels of abstraction (e.g. low-level features capture basic characteristics of the data, while higher-level features capture more complex patterns and relationships). This process is known as representation learning, and the obtained feature vector is recorded as an embedding (Xia et al. 2021). Therefore, it is worth exploring the calculation of the embedding of various scales as a representation closer to the spatial cognition information through deep learning to conduct GSM_ST. Unlike regular data, such as one-dimensional vectors (e.g. voice data) and two-dimensional matrices (e.g. image data), vector data is an irregular structure similar to graph data (Zhang and Guilbert 2012; Yu et al. 2022). Thus, graph neural networks designed to process graph data are more suitable for handling vector data. These networks have been applied to graph similarity measurement through supervised and unsupervised learning. Given the uncertainty of GSM_ST, it will take substantial human resources to construct a batch of samples with accurate similarity labels, making unsupervised learning more favorable in this study. The Graph Auto-Encoders (GAE) (Kipf and Welling 2016) is a representative and general unsupervised model that has been applied to e.g. building shape matching (Yan et al. 2021).

A drainage network is a typical geographic object that needs multi-scale representations. Its GSM_ST has a substantial impact on other geographic elements during scaling transformation.

This is due to their close relationship, such as the connection between rivers and bridges, the parallel attachment between rivers and roads (Thomson and Brooks 2002), the boundary proximity between rivers and buildings (Ai et al. 2015), and the concave and convex matching between rivers and contours (Ai 2007)). Hence, current studies of GSM_ST primarily focus on drainage networks, approached from different perspectives of the global morphological structure (Zhang and Guilbert 2016) or the local geometric detail (Stanislawski et al. 2009; Yan and Li 2015; Yan 2022). To tackle the uncertainty of GSM_ST, this study considers drainage networks as an example and introduces *a GAE model that integrates drainage network characteristics* (DNC_GAE) to perform GSM_ST. First, a drainage graph integrating geometric knowledge using a dual graph was constructed by building the graph edges through the relationship of reaches, and then introducing five morphological characteristics as the node features. Second, the DNC_GAE architecture was designed with the drainage graph as input. Finally, the GSM_ST was performed using the Cosine similarity based on the drainage embeddings of different scales derived from the DNC_GAE encoder.

This study has four highlights:

(1) The GAE model is integrated with the existing drainage knowledge to conduct GSM_ST.
(2) The unsupervised learning method GAE is used to address the uncertainty present in geographic information science and to overcome the limitation of insufficient vector samples.
(3) The DNC_GAE is compared to three other representation learning methods, the GAE using coordinate representation learning, the GAE using Fourier shape descriptor, and the rule-based method.
(4) Objective evaluation of the GSM_ST scheme implemented by the DNC_GAE and other methods is achieved through questionnaires on 71 testing drainage cases.

The remainder of this paper is organized as follows: Section 2 briefly reviews related studies on GSM_ST of drainage networks and the application of graph neural networks in similarity measurement; Section 3 introduces a general DNC_GAE framework for the GSM_ST; Section 4 introduces the experimental data and carries out experimental results analysis, method comparison, and discussion; Section 5 concludes the paper.

2. Literature review

2.1. GSM_ST of drainage networks

The irregularity and complexity of drainage networks, resulting from natural factors such as soil, bedrock, climate, vegetation, and tectonic movement (Howard 1967; Argialas, Lyon, and Mintzer 1988; Kimberling et al. 2012), contrasts with the simplicity of road networks. As a result, current GSM_ST studies primarily focus on drainage networks, which can be classified into two categories.

The first category measures coincidence degree based on a metric derived from river length using the spatial overlay idea. Stanislawski (2009) proposed the coefficient of line correspondence (CLC) by constructing river buffers before and after scaling transformation, counting the overlap, deletion, and mismatch lengths, and using the proportion of the overlap length as the coincidence degree. However, buffer intersection analysis is computationally intensive and prone to errors in high-density vector datasets. Stanislawski, Buttenfield, and Doumbouya (2015) improved the CLC using grid computing instead of vector computing for better performance. Furthermore, to understand the similarity of drainage networks at all grades, Fahrul et al. (2020) introduced an element-matching model (Tversky 1977) based on drainage network coding (e.g. Shreve (Shreve 1966), Strahler (Strahler 1957)) to calculate the CLC of drainage networks at different levels from 1:5,000–1:25,000. However, this approach only considers length or buffer area without considering the topological relationship and spatial morphology of drainage networks, which is a limitation in a GSM_ST perspective.

In the second category, the GSM_ST is realized by calculating the weighted sum of multi-dimension characteristics of drainage networks. Yan and Li (2015) constructed a hierarchical drainage network structure with the river entity as a unit and calculated the weighted average to achieve the similarity measurement using multi-dimensional information, such as geometric characteristics, topological relation, distance relation, and hierarchical relation. Meanwhile, Yang and Wang (2021) employed shape, structural, and distribution characteristics for GSM_ST. Yan, Shen, and Li (2016) and Yan (2022) developed a curve-fitting function of scale and GSM_ST value to meet the similarity requirements for drainage generalization. However, this method overlooks the similarity of the global morphological structure. Zhang and Guilbert (2016) attempted to address this issue by calculating the membership degree of drainage patterns based on the fuzzy logic method, considering geometric features. However, due to the subjective interpretation of spatial cognition of morphological structure, differences in hydrological background knowledge, and the complexity of feature expression, it is difficult to choose one or more features to map the spatial cognition information of drainage morphology directly to address the uncertainty of GSM_ST. Also, the weighted sum method based on limited artificial features is not a robust solution, particularly due to the subjectivity in weight setting.

Moreover, the examination of drainage networks for similarity is also explored from the perspectives of hydrology and geology. For example, Roberts (2019) employed a cross-wavelet spectral transformation of longitudinal river profiles to identify the scales of similarity between drainage networks with a unified scale-dependent perspective of landscape evolution. Bajracharya and Jain (2022) proposed an unsupervised learning approach that utilizes width function and hypsometry to analyze hydrologic conditions in watersheds for identifying hydrologic similarity. However, there is a significant difference in the geometric similarity of drainage networks during scaling transformation in map space associated with spatial cognition (Gao and Cao 2021).

2.2. Application of graph neural networks in similarity measurement

Graph neural networks can be applied to measure graph similarity through two approaches. The first approach uses supervised learning for end-to-end graph similarity measurement by utilizing the graph- or node-level interactive information, which relies on samples with binary labels. Commonly used representatives of this type of network are GNN-CNNs (Bai et al. 2018; Bai et al. 2019) and Siamese GNNs (Liu et al. 2019; Ma et al. 2019), and they have been applied in various fields, such as chemical structure matching (Bai et al. 2018), procedure structure error detection (Li et al. 2019), spatial similarity evaluation of linear objects (Li, Yan, and Lu 2022), and brain connection simulation (Ma et al. 2017). The second approach trains an encoder and decoder through unsupervised graph reconstruction learning, where the encoder generates an embedding of the input graph, and the decoder uses it to reconstruct the graph. Cosine similarity and Euclidean distance are typically used as similarity measurement tools, taking the embedding as inputs. One such method is GAE (Kipf and Welling 2016), which is based on auto-encoders and generates latent representations of undirected graphs; GAE can be used more generally compared to attributed node-level embedding (AE), attributed social network embedding (ASNE) (Rozemberczki, Allen, and Sarkar 2021), and multi-scale attributed node-level embedding (MUSAE) (Liao et al. 2018), which are designed specifically for graph embedding in social networks. For instance, Yan et al. (2021) used GAE to combine multiple building features and produce a reasonable shape representation for building shape matching. Yu and Huang (2022) employed GAE for driving trajectory anomaly detection.

3. Methodology

3.1. Methodology framework

The framework for our geometric similarity measurement method consists of the following three parts (Figure 1):

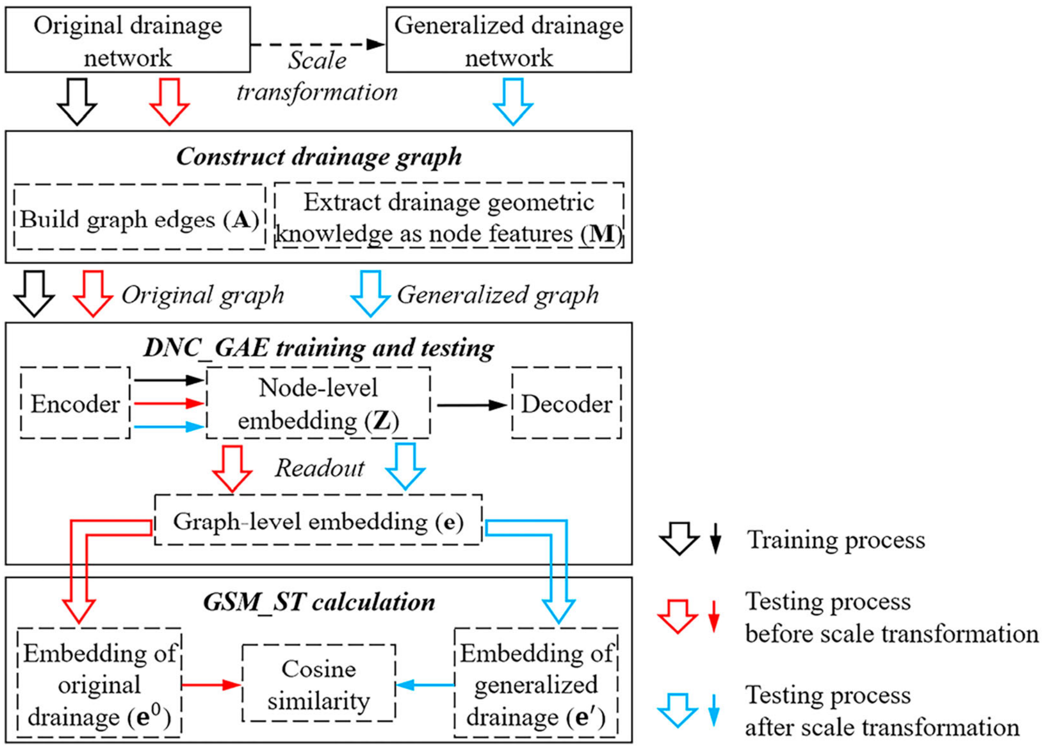

Figure 1. Overall framework for GSM_ST implemented by the DNC_GAE method.

(1) Construct a drainage graph by mapping the connected relationships between reaches as graph edges (represented by the adjacency matrix **A**) and the midpoints of reach as graph nodes. The node features are defined by the drainage geometric knowledge (represented by the feature matrix **M**).
(2) Design, train, and test the DNC_GAE. The encoder takes the drainage graph (matrix **A** and **M**) as input and outputs the node-level embedding **Z**. The decoder takes **Z** as the input to reconstruct the graph edges. During the testing, the node-level embedding **Z** is reduced to the graph-level embedding **e** through a readout function. This procedure is run twice in the testing phase, once for the original network and once for the generalized network.
(3) Calculate the GSM_ST value using Cosine similarity with the drainage embeddings before and after scaling transformation (represented by $\mathbf{e}^0$ and $\mathbf{e}'$, respectively) as inputs.

3.2. Construction of drainage graph

A drainage network can be represented as a directed graph structure, as shown in Figure 2 (a), with sources, junctions, and outlets as nodes and reaches with flow direction as the directed edges. However, the nodes and edges, used to store features and the connection relationship separately, are more widely adopted in graph neural networks (Zhao et al. 2020; Yan et al. 2021). Thus, a dual graph is selected to construct the drainage graph, represented as $G = (\boldsymbol{V}, \boldsymbol{E})$, where $\boldsymbol{V} = \{\boldsymbol{v}_0, \boldsymbol{v}_1, \cdots \boldsymbol{v}_n\}$ is the set of nodes and $\boldsymbol{E}$ is the set of edges. Here, n is the number of reaches and $\boldsymbol{e}_{ij} = (\boldsymbol{v}_i, \boldsymbol{v}_j) \in \boldsymbol{E}$ is the edge connecting $\boldsymbol{v}_i$ and $\boldsymbol{v}_j$.

3.2.1. Construction of graph nodes based on drainage network characteristics

The nodes of the drainage graph correspond to the reaches and contain the geometric shape knowledge. The midpoints of reaches are extracted as the node (red points in Figure 2 (b)), recorded in $\boldsymbol{V}$;

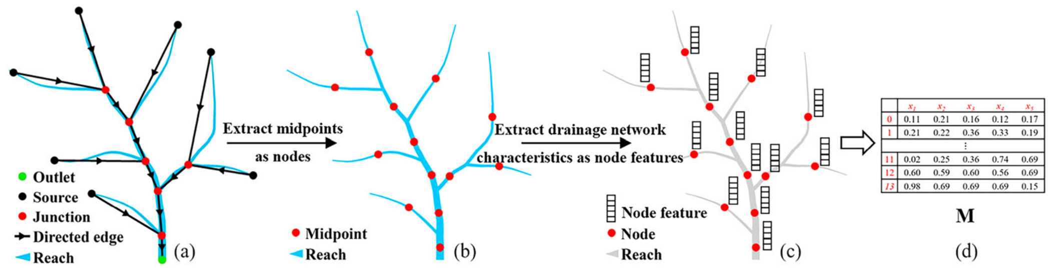

Figure 2. Process of constructing the nodes based on drainage network characteristics (a) a drainage network and its directed graph; (b) midpoints of reaches; (c) node feature construction; (d) feature matrix **M.**

Node features, representing the geometric knowledge, are then constructed (as shown in Figure 2 (c)) to form the feature matrix $\mathbf{M} \in \mathbb{R}^{n\times d}$ (depicted in Figure 2 (d)), where d is the dimension of the node feature and represents the number of drainage network characteristics. These characteristics are derived from mapping the network's geometric characteristics and interconnected structures of reaches (Mejia and Niemann 2008; Bouramtane et al. 2020). Five drainage network characteristics are used for the node features (shown in Table 1), both from the global and local perspectives. For details on these characteristics, see Yu et al. (2022).

3.2.2. Construction of graph edges

Building on the nodes constructed in the previous section (see Figure 4 (a)), they are then connected based on the inflow relationship between reaches (see Figure 4 (b)). For instance, in Figure 4 (b), both reach $\boldsymbol{i}$ (mapped as the $\boldsymbol{v}_i$) and reach $\boldsymbol{j}$ (mapped as the $\boldsymbol{v}_j$) flow together to reach $\boldsymbol{k}$ (mapped as the $\boldsymbol{v}_k$), so $\boldsymbol{v}_i$, $\boldsymbol{v}_j$, and $\boldsymbol{v}_k$ should be connected following $\boldsymbol{v}_i - \boldsymbol{v}_j - \boldsymbol{v}_k - \boldsymbol{v}_i$ to form the $\boldsymbol{e}_{ij}$, $\boldsymbol{e}_{jk}$, and $\boldsymbol{e}_{ik}$. Finally, the connection relationship between the nodes is recorded as the adjacency matrix $\mathbf{A} \in \mathbb{R}^{n\times n}$ (see Figure 4 (d)), where $\mathbf{A}_{ij} = 1$ if there is an edge $\boldsymbol{e}_{ij}$ connecting $\boldsymbol{v}_i$ and $\boldsymbol{v}_j$ or $\mathbf{A}_{ij} = 0$ if there is no such edge.

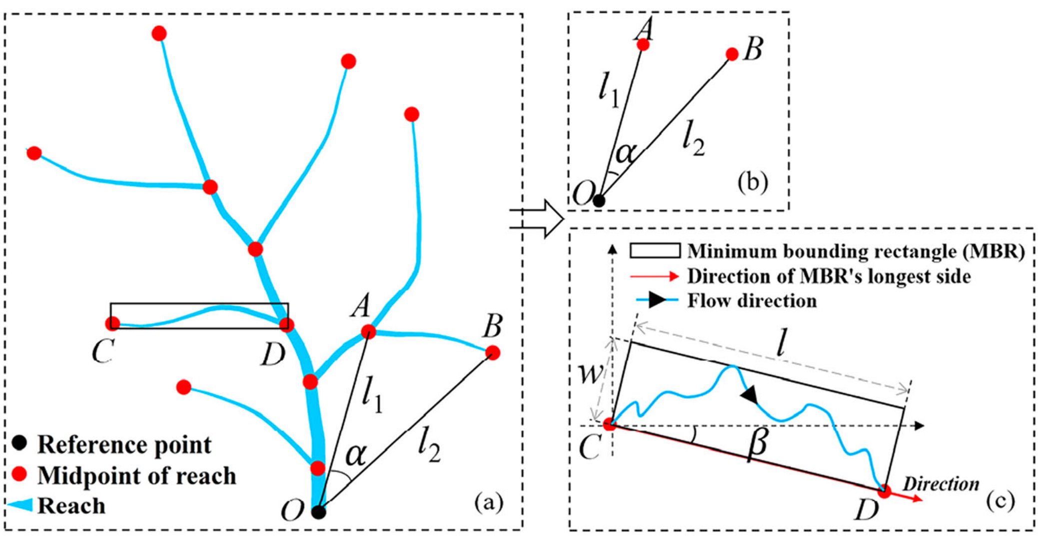

Figure 3. (a) Schematic diagram of calculation of the drainage network characteristics; (b) schematic diagram of reference point distance difference and angle; (c) schematic diagram of the length-width ratio of MBR and direction of the MBR longest side (β).

Table 1. Five drainage network characteristics from the global and local views used as the node features.

Views	Characteristics	Description
Global view	Reference point distance difference	The difference between the Euclidian distance between the endpoints of the reach curve and the reference point ($l_1 - l_2$ in Figure 3 (b))
	Reference point angle	The angle formed by the endpoints of the reach curve and the reference point (α in Figure 3 (b))
Local view	Curve length of a reach	–
	The breadth-length ratio of the minimum bounding rectangle (MBR)	The reciprocal of the length-width ratio of the MBR of a reach ($\frac{l}{w}$ in Figure 3 (c)) (Davis 1991)
	The direction of the MBR's longest side	The direction of the longest side of the MBR of the reach (solid red arrow (β) in Figure 3 (c))

3.2.3. Combination of the drainage graph edges and nodes

The drainage graph is built by combining the nodes and edges (see Figure 5 (a)). Each node records 5-dimensional features, and the edges connect them according to the connection between reaches in the spatial visualization. Finally, the graph is represented as the adjacency matrix **A** and the feature matrix **M** (as shown in Figure 5 (b)), which serve as inputs for DNC_GAE.

3.3. Graph autoencoder network

GAE maps the input graph into a new vector space, denoted as an embedding, which can be regarded as the vectorization of the spatial cognition of a drainage network. It consists of an encoder and a decoder (see Figure 6). The encoder takes the drainage graph (**M**, **A**) as input to calculate the node-level embedding ($\mathbf{Z} \in \mathbb{R}^{n \times m}$, where n is the number of nodes and m represents the dimension of node features) (Section 3.3.1). The decoder takes the **Z** as inputs to reconstruct the edges ($\mathbf{A}' \in \mathbb{R}^{n \times n}$) (Kipf and Welling 2016), with the goal of minimizing the difference between the reconstructed adjacency matrix $\mathbf{A}'$ and the original adjacency matrix **A** (Section 3.3.2). During the testing process, the **Z** is reduced to a graph-level embedding $\mathbf{e} \in \mathbb{R}^{1 \times m}$ using a mean readout function, which is then used for the Cosine similarity calculation (Section 3.4).

In the scaling transformation of a drainage network, the number of nodes at a large scale is greater than at a small scale. A GAE trained by semi-supervised transductive learning based on a large graph is not applicable to other drainage cases with varying numbers of reaches. Therefore, this study trains the DNC_GAE through unsupervised inductive learning, which can handle drainage graphs with varying numbers of nodes.

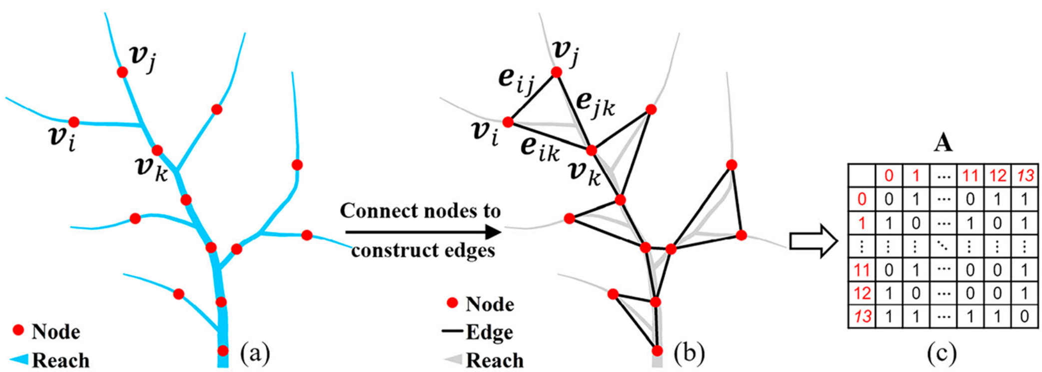

	0	1	···	11	12	13
0	0	1	···	0	1	1
1	1	0	···	1	0	1
⋮	⋮	⋮	⋱	⋮	⋮	⋮
11	0	1	···	0	0	1
12	1	0	···	0	0	1
13	1	1	···	1	1	0

Figure 4. Process of constructing graph edges. (a) reaches and drainage graph nodes; (b) connect the nodes to construct the edges; (c) adjacency matrix **A**.

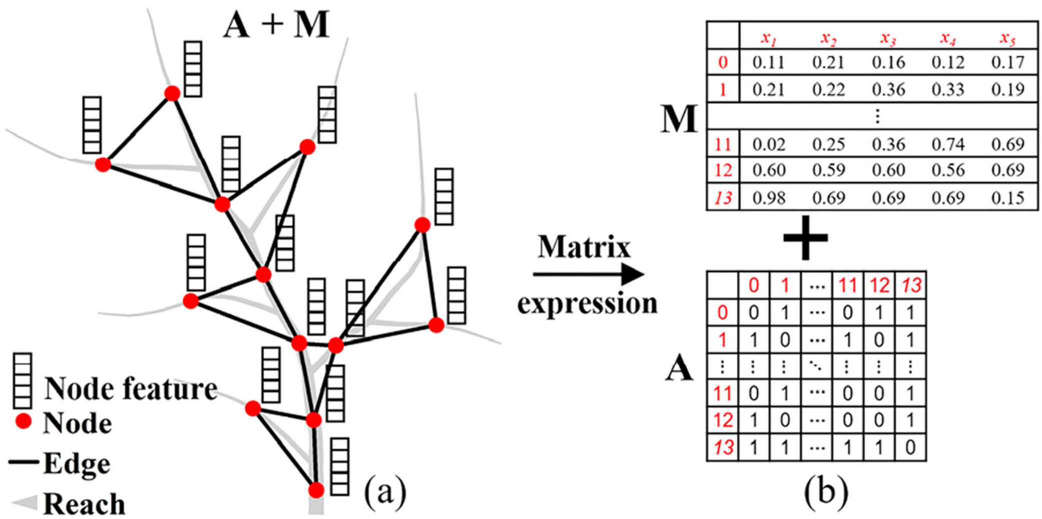

Figure 5. Combination of the edges and nodes with matrix expression as the adjacency matrix **A** and the feature matrix **M**.

3.3.1. DNC_GAE encoder

The encoder is fed the drainage graph ($\mathbf{M}$, $\mathbf{A}$) to calculate the node-level embedding level $\mathbf{Z} \in \mathbb{R}^{n\times m}$ (see Figure 7 (a)):

$$\mathbf{Z} = GCNN(\mathbf{M}, \mathbf{A}) \tag{1}$$

where $GCNN(\cdot)$ denotes the 1st-ChebNet (Kipf and Welling 2017). As shown in Figure 7 (b), the encoder consists of 1st-Chebyshev graph convolution layers. Each layer output is as follows:

$$\mathbf{H}^{l+1} = \sigma\left(\tilde{\mathbf{D}}^{-\frac{1}{2}}\tilde{\mathbf{A}}\tilde{\mathbf{D}}^{-\frac{1}{2}}\mathbf{H}^{l}\mathbf{W}^{l} + \mathbf{b}^{l}\right) \tag{2}$$

where $\mathbf{H}^{l+1} \in \mathbb{R}^{n\times m_{l+1}}$ is the convolved signal matrix in the $(l+1)^{th}$ layer, where m_{l+1} is the dimension of the node features in the $(l+1)^{th}$ layer and $\mathbf{H}^0 = \mathbf{M}$. Besides, $\tilde{\mathbf{D}}$ is a degree matrix of $\tilde{\mathbf{A}}$, where $\tilde{\mathbf{A}} = \mathbf{A} + \mathbf{I}_n$, and $\tilde{\mathbf{D}}_{ii} = \sum_j \tilde{\mathbf{A}}_{ij}$. Here, $\mathbf{I}_n \in \mathbb{R}^{n\times n}$ is the identity matrix. $\mathbf{W}^l \in \mathbb{R}^{m_l\times m_{l+1}}$ and $\mathbf{b}^l \in \mathbb{R}^{1\times m_{l+1}}$ are the training weight and common bias of the l^{th} layer, respectively. $\sigma(\cdot)$ denotes the activate function, where $\sigma(\cdot)$ of the hidden layers is the rectified linear unit function

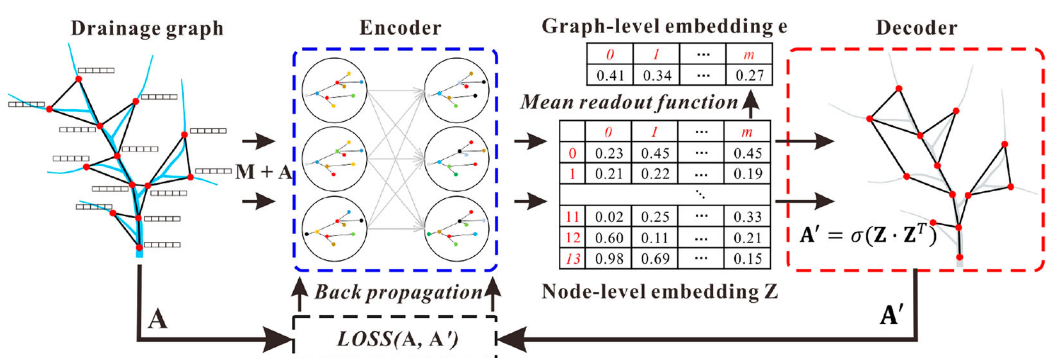

Figure 6. DNC_GAE architecture.

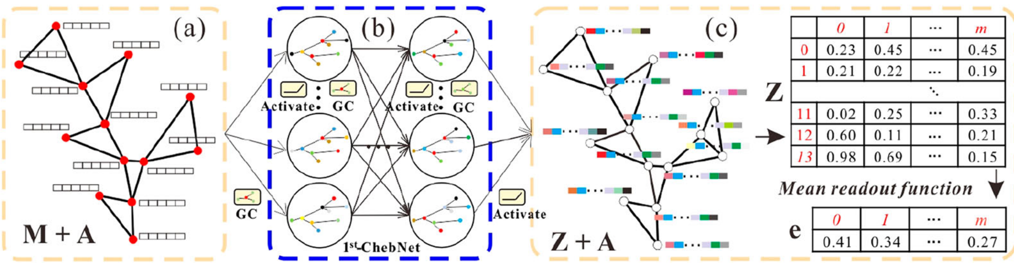

Figure 7. DNC_GAE encoder (a) a drainage graph; (b) 1st-ChebNet; (c) Node-level embedding **Z** and graph-level embedding **e**; GC: graph convolution.

Relu(·) and $\sigma(\cdot)$ of the output layer is the logistic sigmoid function *sigmoid*(·). For details, please see Kipf and Welling (2016).

The encoder outputs the node-level embedding, but GSM_ST requires the graph-level embedding. Usually, the conversion from the node-level embedding to the graph-level embedding is realized through a readout function, such as mean, max (Duvenaud et al. 2015; Atwood and Towsley 2016), or pooling (Ying et al. 2018). In this study, the node-level embedding from the encoder contains the information from the adjacent nodes through the information transmission based on edge implemented by graph convolution, resulting in a high coincidence of the information between the nodes (Ying et al. 2018; Zhang et al. 2019). Therefore, the mean operator is chosen to convert the node-level embedding $\mathbf{Z} \in \mathbb{R}^{n\times m}$ to the graph-level $\mathbf{e} \in \mathbb{R}^{1\times m}$ (see Figure 7 (c)).

3.3.2. DNC_GAE decoder and loss function

During DNC_GAE training, the high coincidence between the adjacent nodes in the node-level embedding $\mathbf{Z}$ helps reconstruct the relationship between nodes (Kipf and Welling 2016). This leads to the design of the decoder, rebuilding the connection between nodes (recorded as $\mathbf{A}'$) based on $\mathbf{Z}$. The accuracy of the node-level embedding $\mathbf{Z}$ can be measured by the distance between $\mathbf{A}'$ and $\mathbf{A}$. Therefore, the DNC_GAE aims to minimize this difference, calculated by the cross entropy loss function without using label samples, thus achieving unsupervised learning.

3.4. GSM_ST based on the graph-level embedding

The graph-level embeddings of a drainage network, denoted as $\mathbf{e}$, are recorded as $\mathbf{e}^0$ and $\mathbf{e}'$ before and after scaling transformation, respectively. Therefore, GSM_ST is regarded as the similarity (*sim*) between two high-dimensional vectors, which is conducted by the Cosine similarity:

$$sim = \frac{\mathbf{e}^0 \cdot \mathbf{e}'}{\mathbf{e}^0\mathbf{e}'} = \frac{\sum_{i=1}^{m} \mathrm{e}_i^0 \times \mathrm{e}_i'}{\sqrt{\sum_{i=1}^{m} (\mathrm{e}_i^0)^2} \times \sqrt{\sum_{i=1}^{m} (\mathrm{e}_i')^2}} \tag{3}$$

4. Experiments and analysis

In this section, we present the experiment data (Section 4.1), conduct the hyperparameter sensitivity experiments (Section 4.2), and analyze the DNC_GAE learning process (Section 4.3). Besides, we compare its performance against other representation learning methods and GAE with different features through a questionnaire (Section 4.4). Lastly, we analyze the GSM_ST result supported by the DNC_GAE and discuss its benefits over the traditional method (Section 4.5).

4.1. Experimental data

4.1.1. Original drainage network data

The original drainage network data used for experiments was obtained from the National Hydrography Dataset (NHD) of USGS (https://apps.nationalmap.gov) at a scale of 1:24,000, specifically the NHDFlowline data. The drainage cases were segmented by the 10-level watershed data from the USGS Watershed Boundary Dataset (https://www.usgs.gov/national-hydrography/watershed-boundary-dataset), which contained eight levels of progressive hydrologic units identified by unique 2- to 16-levels. The experimental drainage networks covered 28 states (see Figure 8). Besides, the original drainage network data underwent some pretreatment operators, such as deleting the single reach, revising the flow, and processing the looping river. In total, 771 drainage cases were collected, with the number of nodes ranging from 85 to 1648. These cases were then divided into 650 training samples, 50 validating samples, and 71 testing samples.

4.1.2. Generalized drainage network data

In the experiment, drainage network selection was used to achieve scaling transformation. Specifically, Horton coding was first constructed based on strokes of the drainage network. Then, the number of strokes after the selection was calculated using the square root law (Töpfer and Pillewizer 1966). Finally, strokes were selected according to the length of strokes, starting from the high grade of Horton coding (Mazur and Castner 1990). The original drainage networks (in scale 1:24,000)

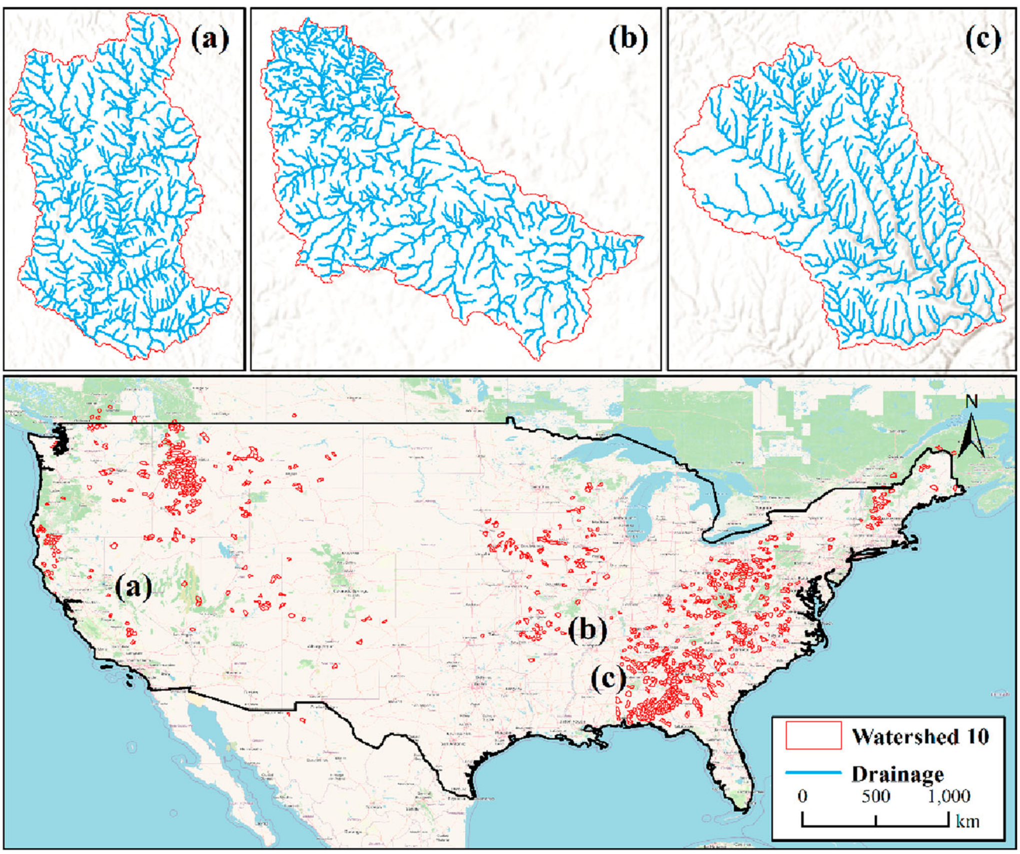

Figure 8. Spatial distribution of the original drainage networks. The three shown drainage networks are in Nevada (a), Missouri (b), and Alabama (c). Source of hillshade: http://goto.arcgisonline.com/maps/Elevation/World_Hillshade.

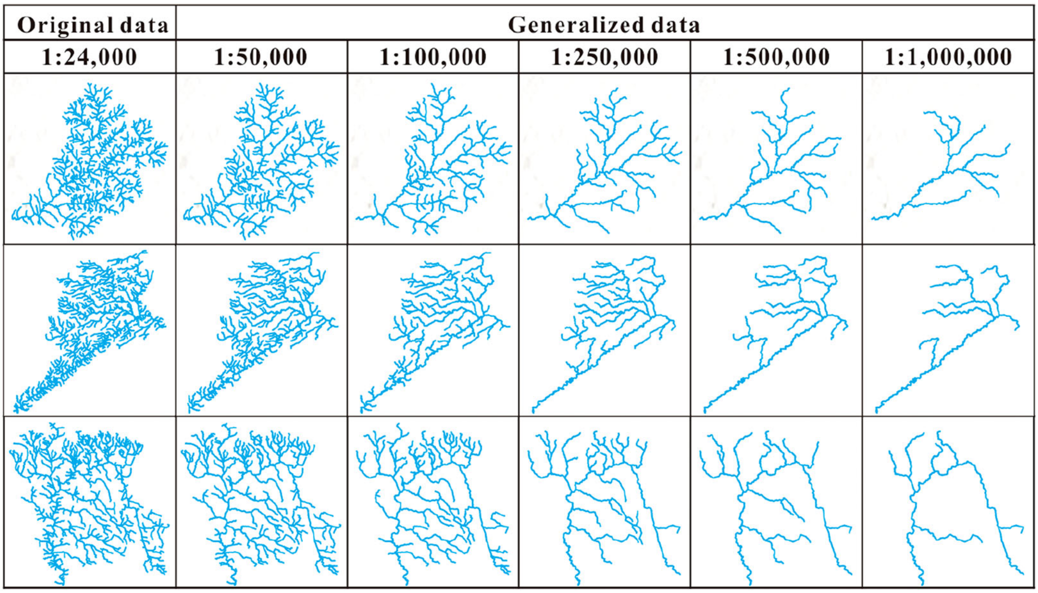

Figure 9. Diagram of the original drainage networks at a scale of 1:24,000 and the generalized drainage networks at 1:50,000, 1:100,000, 1:250,000, 1:500,000, and 1:1,000,000.

were generalized in the number of strokes to the target scales: 1:50,000, 1:100,000, 1:250,000, 1:500,000, and 1:1,000,000 (see Figure 9). Note that the geometry of the reaches was not simplified.

4.2. Hyperparameter sensitivity analysis

A deep learning model often has many hyperparameters significantly impacting the model's efficiency. The DNC_GAE hyperparameters include the number of graph-convolutional layers (GCLs) (see Figure 7 (b)), learning rate (LR), and embedding size (ES) referred to m in Figure 7 (c). In this section, we conducted hyperparameter sensitivity experiments to analyze the effects of different hyperparameter combinations to determine the optimal settings. The candidate values for the hyperparameters were selected from commonly used values: GCLs = {2, 3, 4}, LR = {0.01, 0.001, 0.0001}, and ES = {16, 32, 64, 128, 256}. Figures 10–12 display the validation loss curves for all 45 groups for hyperparameter combinations, allowing for visualization of the model-fitting effect.

According to Figure 10, increasing GCLs while keeping LR and ES constant improves the speed and efficiency of the model fitting. When GCLs = 4 (see the red curve in Figure 10 except for Figure 10 (j) and (n)), the model performs best in any combination of LR and ES. This suggests that GCLs = 4 is the optimal hyperparameter among the candidates.

Figure 11 shows that a larger ES results in a faster decrease in the loss curve and lower validation loss in general. The purple curve in Figure 11 (except for the subgraphs (b) and (c)) demonstrates that 256 is the best ES among the candidates.

From the perspective of LR, when GCLs and ES are set in a 'high-high' manner (see Figure 12 (h), (i), (k), (l), (m), and (o)), too low LR (LR = 0.0001) leads to underfitting and too high LR (LR = 0.01) causes the model to fail to fit (as seen in the red curves in Figure 12 (l), (m), and (o)). If GCLs and ES are not set in the 'high-high' manner, the model fitting improves with an increase in LR, as shown in the red curves of Figure 12 (a), (b), and (c), etc.

Combining the optimal hyperparameters of GCLs = 4 and ES = 256, the optimal LR should be 0.001. This group of hyperparameter values also realizes the best performance, as evidenced by

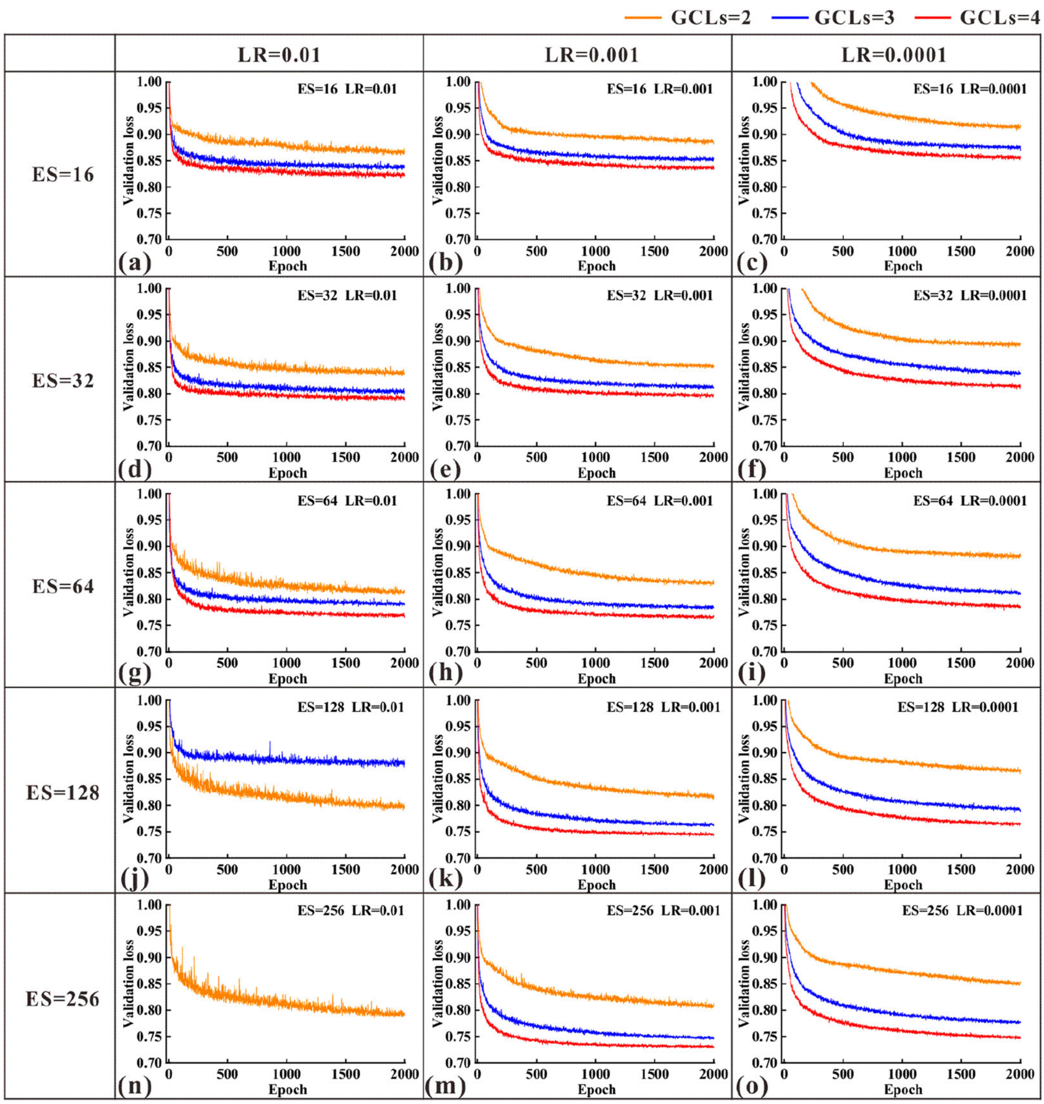

Figure 10. Training process from GCLs perspective. GCLs: the number of graph-convolutional layers.

the red curve in Figure 10 (m), the purple curve in Figure 11 (f), and the blue curve in Figure 12 (o)). Therefore, the hyperparameter group of GCLs = 4, ES = 256, and LR = 0.001 is selected for the subsequent experiments with the DNC_GAE.

4.3. GSM_ST learning result

This section describes the learning process of the GSM_ST implemented by DNC_GAE. The process involves calculating loss and determining Precision, Recall, F1-score, and Area Under Curve (AUC) based on positive and negative edges of 50 validation graphs. Positive edges are those present in the graph, while negative edges are randomly generated and equal in number to positive ones. Precision and Recall measure the accuracy of the reconstructed positive edges, while F1-score and AUC assess the DNC_GAE's ability to reconstruct the graph, reflecting the correctness

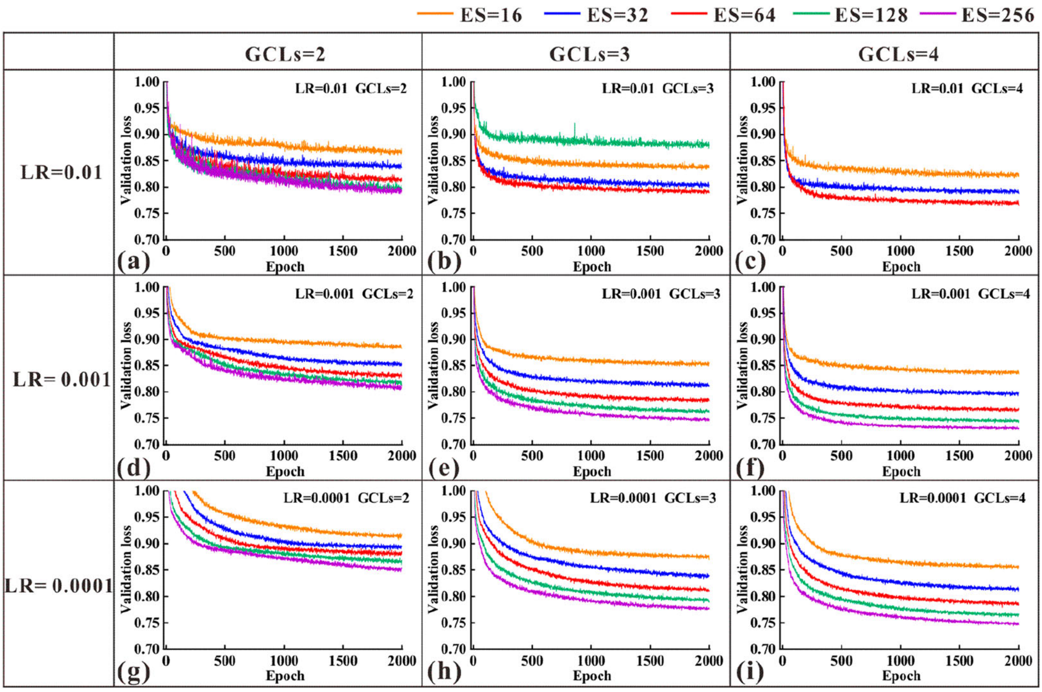

Figure 11. Training process from ES perspective. ES: embedding size.

of the node-level embedding **Z** and graph-level embedding **e** derived from the DNC_GAE encoder.

As illustrated in Figure 13, the training and validation losses decrease rapidly and then stabilize around 1000 epochs. This demonstrates the efficient performance of the DNC_GAE on both training and validation data without significant overfitting. Meanwhile, the Precision and Recall gradually increase and remain steady at 0.98. This indicates that DNC_GAE achieves good accuracy in reconstructing the positive edges. Furthermore, the AUC and F1-score rise, then stabilize at 0.99 and 0.98, respectively, demonstrating the DNC_GAE's stable and correct reconstruction of the graph. The results suggest that the node-level embeddings **Z** and the graph-level embeddings **e** generated by the encoder are correct and efficient, leading to a well-fitting model that authentically represents the drainage morphology. This can serve the subsequent GSM_ST analysis.

4.4. Evaluation

To validate the effectiveness of the DNC_GAE, two studies were performed: (1) a contrast experiment between the DNC_GAE and alternative representation learning methods; (2) a questionnaire to compare the performance of DNC_GAE with different methods.

4.4.1. Comparison with other representation learning methods

The contrast experiment utilized several representation learning methods for conducting GSM_ST, including AE, ASNE, and MUSAE (cf. Section 2.2). These three methods, taking the drainage graph as input, performed representation learning to obtain the graph-level embeddings that were then used to compute the Cosine similarity. Figure 14 shows a visualization of scaling transformation and the GSM_ST results for the four drainage cases. Noticeably, the GSM_ST values of AE and MUSAE are severely out of the normal range and do not show a corresponding decrease with

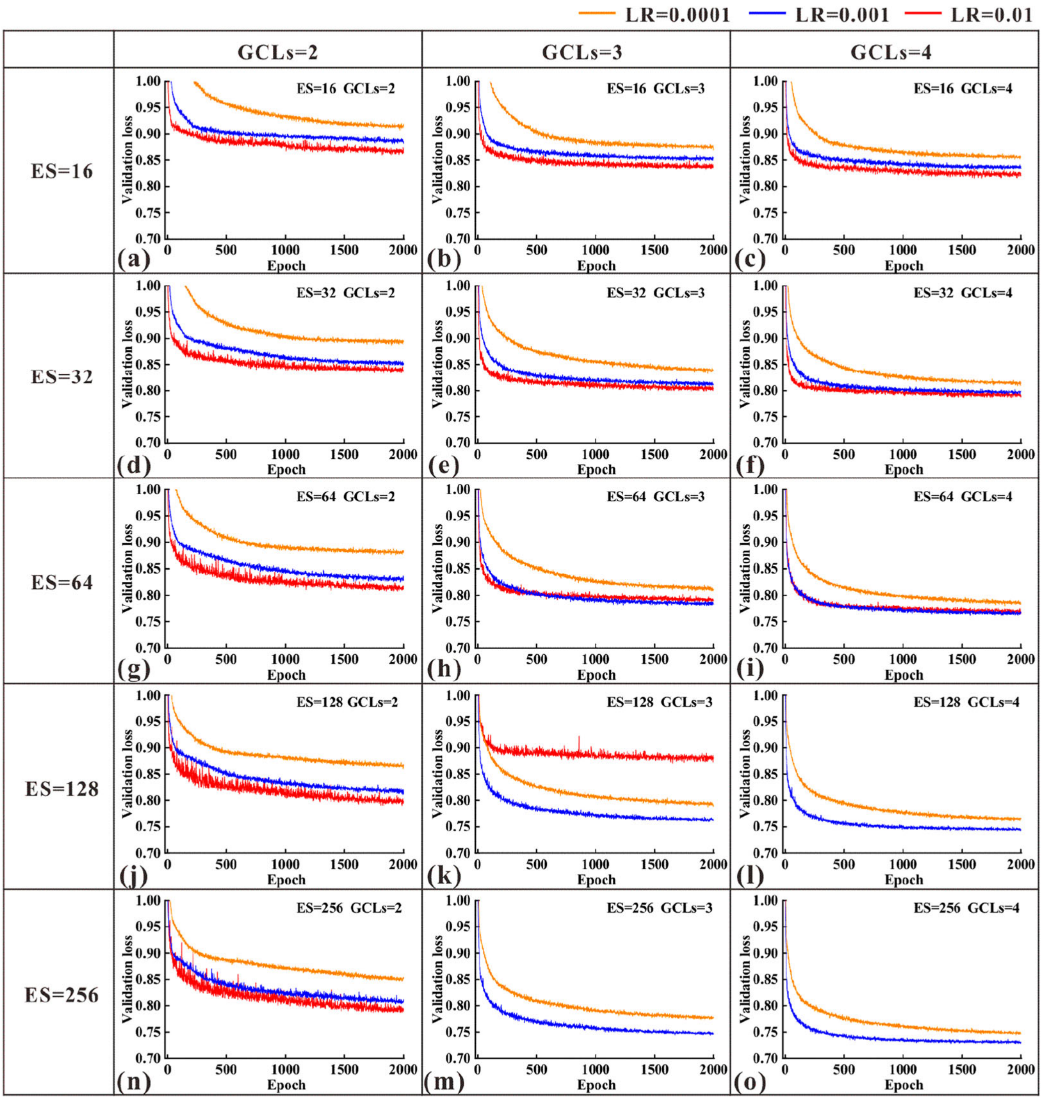

Figure 12. Training process from LR perspective. LR: learning rate.

decreasing scale. For example, the GSM_ST values of AE and MUSAE at all scales are above 0.9, which contradicts spatial cognition, where drainage morphology gradually generalizes. Moreover, the ASNE values show some decay but are still excessively high at small scales, which does not align with the greatly abstract spatial cognition of the drainage network morphology. For instance, the minimum value of ASNE at a scale of 1:1,000,000 is 0.4554, significantly higher than the expected range. Conversely, the GSM_ST scheme implemented by the DNC_GAE is more reasonable and declines with decreasing scale, with high values at large scales and low values at small scales, consistent with the spatial cognition of drainage morphology.

In general, the aforementioned representation learning methods, including AE, ASNE, and MUSAE, struggle to achieve acceptable results in the GSM_ST when applied to the drainage graphs. Compared to DNC_GAE, their performance is inferior. It is worth noting that AE, ASNE, and MUSAE are specific graph embedding techniques designed to learn node representations in social networks, taking into account the varying sizes and information within each node (Liao et al. 2018;

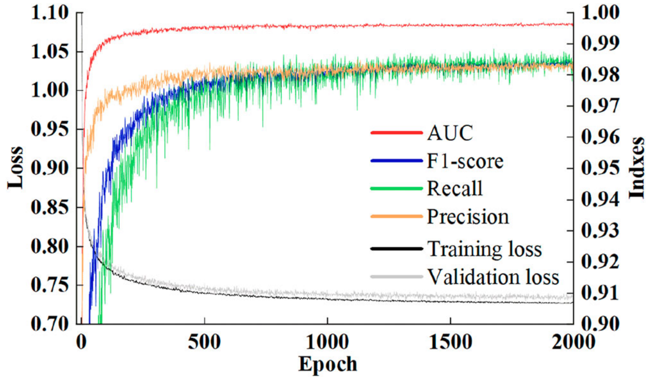

Figure 13. Changes curve of training loss, validation loss, Precision, Recall, F1-score, and AUC during the learning process of DNC_GAE.

Table 2. Opinion statistics (**Q**) of 23 interviewees on 65 GSM_ST cases using DNC_GAE, FSD_GAE, CE_GAE, and SIM_global. (DNC_GAE is our proposed method; FSD_GAE is the GAE using Fourier shape descriptor; CE_GAE is the GAE using coordinate embedding; SIM_global is a typical traditional method).

Method	Agree	Disagree	Uncertainty	Satisfaction ratio
DNC_GAE	57	6	2	87.69%
FSD_GAE	34	30	1	52.31%
CE_GAE	13	47	5	20.00%
SIM_global	5	57	3	7.69%

Rozemberczki, Allen, and Sarkar 2021). On the other hand, GAE is a more general method for learning graph embeddings, considering the same feature size and information within each node. In the drainage graph, node features are characterized by the five drainage network characteristics, resulting in uniformity in features. This uniformity mainly contributes to the superior performance of the usage of GAE in the GSM_ST compared to other methods.

4.4.2. Evaluation method of GSM_ST – Questionnaire

Human cognition of shape is a combination of logical and pictorial thinking. To evaluate any model's shape similarity recognition results, human perception must be considered (Liu et al. 2022). In this study, the evaluation was performed by sending questionnaires to 25 individuals, of whom 23 responded. There were 14 men and nine women, of whom eight were practitioners in the geography information science industry and the remaining 15 were masters or doctoral students in geographic information science. Respondents ranged in age from 23 to 35.

Apart from our method, the questionnaire included the GAE using Fourier shape descriptor (FSD_GAE), the GAE using coordinate embedding (CE_GAE), and SIM_global (Yang and Wang 2021). The FSD_GAE takes the drainage graph as input, with the Fourier shape descriptor of the reach curve ((Liu et al. 2020)) as the node features, while the node features fed into the CE_GAE are the coordinate embedding derived from a Deep Graph Infomax network (Veličković et al. 2018) with the reach coordinates as inputs.

All 71 testing drainage cases (cf. Section 4.1.1) were utilized in the questionnaire survey. The questions in the questionnaire are structured based on two aspects, as illustrated in Figure 15. The first aspect is participants' opinions (categorized as *agree*, *disagree*, and *uncertainty*, represented in blue font in Figure 15) on the GSM_ST results from four methods. The second aspect is selecting the best method in each testing drainage case (see the red font in Figure 15).

Method \ GSM_ST \ Case	1:24,000	1:50,000	1:100,000	1:250,000	1:500,000	1:1,000,000
Case 43	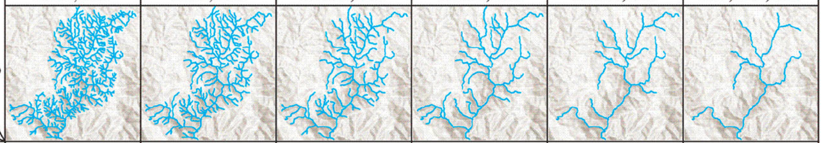					
AE	1.00	0.9787	0.9808	0.9752	0.9863	0.9732
ASNE	1.00	0.8540	0.8020	0.7198	0.7018	0.6824
MUSAE	1.00	0.9435	0.9357	0.9025	0.9163	0.9177
DNC_GAE	**1.00**	**0.7832**	**0.5991**	**0.3764**	**0.3246**	**0.2620**
Case 57	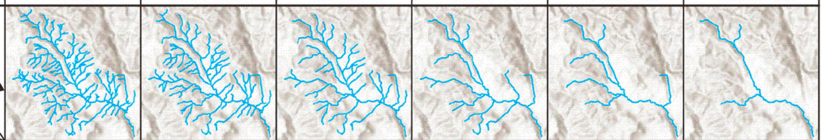					
AE	1.00	0.9748	0.9754	0.9754	0.9745	0.9721
ASNE	1.00	0.8422	0.7781	0.6957	0.6116	0.5247
MUSAE	1.00	0.9573	0.9659	0.9653	0.9692	0.9606
DNC_GAE	**1.00**	**0.8197**	**0.6697**	**0.5608**	**0.3691**	**0.2648**
Case 60	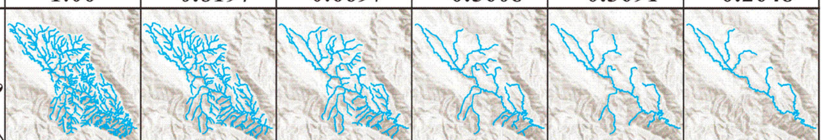					
AE	1.00	0.9632	0.9704	0.9725	0.9836	0.9696
ASNE	1.00	0.8327	0.7889	0.6510	0.6167	0.4554
MUSAE	1.00	0.9149	0.9297	0.9348	0.9343	0.9288
DNC_GAE	**1.00**	**0.7579**	**0.6169**	**0.4725**	**0.3147**	**0.2466**
Case 64	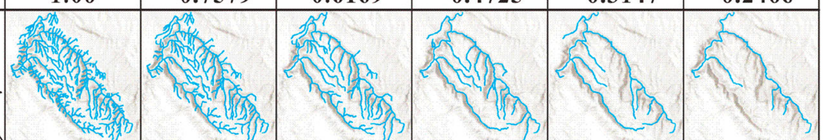					
AE	1.00	0.9434	0.9602	0.9607	0.9533	0.9598
ASNE	1.00	0.8171	0.7242	0.7257	0.6839	0.4641
MUSAE	1.00	0.9478	0.9490	0.9628	0.9652	0.9643
DNC_GAE	**1.00**	**0.7884**	**0.6231**	**0.4695**	**0.3131**	**0.2232**

Figure 14. The GSM_ST results of AE, ASNE, MUSAE, and DNC_GAE. For example, the GSM_ST result for AE at a scale of 1:50,000 exhibits a similarity value (using Cosine similarity) of 0.9787, indicating the degree of similarity between a drainage network (case 43) at scales of 1:24,000 and 1:50,000. The case numbers correspond to those shown in Figures 16 and 17.

Methods \ Similarity \ Cases	1:24,000	1:50,000	1:100,000	1:250,000	1:500,000	1:1,000,000	Questions
	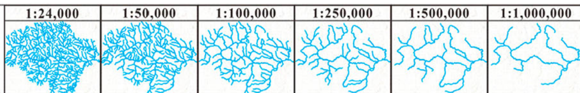						
DNC_GAE	1.00	0.856	0.725	0.550	0.432	0.326	Q1: ○ Agreed ○ Disagree ○ Uncertainty
FSD_GAE	1.00	0.961	0.902	0.815	0.753	0.683	Q2: ○ Agreed ○ Disagree ○ Uncertainty
CE_GAE	1.00	0.955	0.916	0.883	0.789	0.547	Q3: ○ Agreed ○ Disagree ○ Uncertainty
SIM_global	1.00	0.812	0.576	0.696	0.641	0.580	Q4: ○ Agreed ○ Disagree ○ Uncertainty
Best method	Q5: ○ GS_GAE ○ FSD_GAE ○ CE_GAE ○ SIM_global						

Figure 15. Format of the questionnaire used to evaluate the four methods in a single drainage case. The question asked is whether the methods provide an appropriate implementation of GSM_ST. (DNC_GAE is our proposed method; FSD_GAE is the GAE using Fourier shape descriptor; CE_GAE is the GAE using coordinate embedding; SIM_global is a typical traditional method.)

The first six drainage cases were used as an adaptation to familiarize the interviewees with the questionnaire. Therefore, the final statistics and analysis are based on the results of the remaining 65 drainage cases. The first type of question recorded the number of opinions on each of the four methods, represented as $\mathbf{Q} \in \mathbb{R}^{4\times3}$, where 4 is the number of methods and 3 is the number of opinions $\{agree, disagree, uncertainty\}$:

$$\mathbf{Q}_{ij} = \sum_{k=1}^{65} q_j^i k \; (i = 1,\; 2,\; 3,\; 4;\; j = 1,\; 2,\; 3) \tag{4}$$

$$q_j^i k = \begin{cases} 1, & mode(Opinion_k^i) = \; count(Opinion_k^i(j)) \\ 0, & mode(Opinion_k^i) \neq \; count(Opinion_k^i(j)) \end{cases} \tag{5}$$

where $q_j^i k$ denotes a logistic value denoting whether the GSM_ST result of the k^{th} cases implemented by method i gets opinion j; $Opinion_k^i$ represents the opinion on the result of the k^{th} cases using method i and $Opinion_k^i(j)$ was the opinion j of the set $Opinion_k^i$. $count(Opinion_k^i(j))$ is the number of the corresponding opinion j and $count(Opinion_k^i(1)) + \; count(Opinion_k^i(2)) + \; count(Opinion_k^i(3)) = 23$. $mode(Opinion_k^i)$ describes the mode of the $Opinion_k^i$, and $q_3^i k = 1$ if there are two mode values at the same time. Finally, the satisfaction ratio of each method i is calculated as $\frac{\mathbf{Q}_{i1}}{65}$.

4.4.3. Comparison with GAE support by Fourier shape descriptor and coordinate embedding

Section 4.4.1 verified the validity of the GAE applied to GSM_ST. To assess the performance of the drainage network characteristics in GSM_ST, we compared the results of DNC_GAE, FSD_GAE, and CE_GAE using a heatmap based on the evaluation of 23 respondents. Figure 16 displays the opinion of the interviewees on the GSM_ST implemented by each method. The X-axis represents 65 testing drainage cases, and the Y-axis represents the opinions of 23 interviewees on the GSM_ST. Green squares denote 'agree,' red squares denote 'disagree,' and gray squares denote 'uncertainty.' The results show that the DNC_GAE (Figure 16 (a)) received a higher proportion of green squares compared to FSD_GAE (Figure 16 (b)) and CE_GAE (Figure 16 (c)). Table 2 summarizes the maximum opinions of the 23 interviewees in each case, showing that DNC_GAE received agreement in 57 cases with a satisfaction rate of 87.69%, significantly higher than FSD_GAE at 52.31% and CE_GAE at 20.00%. Additionally, Table 3 demonstrates that DNC_GAE outperforms FSD_GAE and CE_GAE in 51 cases, compared to only 9 and 4 cases, respectively. Overall, the results suggest that the DNC_GAE performs better than FSD_GAE and CE_GAE in GSM_ST.

When comparing the GSM_ST schemes for different drainage cases, Figure 17 shows that the CE_GAE achieves too high values, particularly at small and medium scales, which greatly deviates from the spatial cognition of highly generalized drainage morphology. For example, in case 43, the GSM_ST values at scales 1:500,000 and 1,000,000 are 0.6756 and 0.5466, respectively, which are outside the normal range (below 0.4). Similar observations were made for cases 57 and 60. On the other hand, FSD_GAE underestimates the GSM_ST values at large scales. For example, the GSM_ST values for case 60 at scales of 1:50,000 and 1:100,000 are 0.4914 and 0.3433, respectively, as well as case 64 at a scale of 1:100,000. These values deviate greatly from the spatial cognition of the drainage network morphology, maintaining consistency in the global spatial morphology and the density distribution between these scales and the original scale (1:24,000).

Additionally, FSD_GAE suffers from the problem that the GSM_ST value at small scales does not decrease with the gradual generalization of the drainage morphology. For example, in case 64, the GSM_ST value at 1:500,000 is 0.1496, lower than 0.1621 at 1:1,000,000, despite the mainstream containing more information at the former scale. Conversely, the GSM_ST implemented by DNC_GAE appears to be more reasonable, with similarity decreasing with the decrease of

Figure 16. A heatmap of the opinions of 23 interviewees on 65 GSM_ST cases using DNC_GAE, FSD_GAE, CE_GAE, and SIM_global. (DNC_GAE is our proposed method; FSD_GAE is the GAE using Fourier shape descriptor; CE_GAE is the GAE using coordinate embedding; SIM_global is a typical traditional method.)

Table 3. The optimal method statistics from the questionnaire based on 65 drainage cases.

	DNC_GAE	FSD_GAE	CE_GAE	SIM_global
The number of cases selected as the optimal method	51	9	4	1

scale, with high values at large scale and low values at small scale, aligning with the spatial cognition of drainage morphology. In summary, DNC_GAE performs much better than FSD_GAE and CE_GAE in GSM_ST, indicating that the graph using the drainage network characteristics can better support GAE in conducting GSM_ST.

The comparison reveals that both FSD_GAE and CE_GAE have significant shortcomings in the GSM_ST. FSD_GAE is limited by its fixed vector dimension of node features, making it challenging to accurately describe all reaches (with different reach lengths, tortuosity ratios, and coordinates) using the Fourier shape descriptors with various numbers of Fourier expansion terms (Liu et al. 2020). This leads to insufficient information being fed into the GAE. On the other hand, CE_GAE uses coordinate embeddings to store all the shape information of the reach, leading to potential information redundancy and degraded performance. Our proposed method, DNC_GAE, uses a combination of global and local drainage geometric knowledge, selected through sensitivity analysis experiments by Yu et al. (2022), to avoid such redundancies and provide more accurate information for the GSM_ST implemented by GAE.

4.5. DNC_GAE result and discussion

4.5.1. DNC_GAE result

The opinions of 23 respondents regarding the GSM_ST results implemented by the DNC_GAE are displayed in Figure 16 (a). The blocks are predominantly displayed in green, signifying widespread agreement among most respondents on the majority of GSM_ST results implemented by the DNC_GAE. Additionally, more than half of the respondents disagree with the results in only a few cases, such as 3, 16, 21, 31, 38, and 40. After a comprehensive evaluation of the GSM_ST results produced by DNC_GAE through the involvement of 23 respondents to minimize subjective biases and comprehensive testing of 65 drainage cases to enhance the model's robustness, it can be concluded that DNC_GAE yields exceptional GSM_ST results.

Figure 18 shows the result of a visualization analysis of the drainage networks that received the most agreement (drainage_agreed) and disagreement (drainage_disagreed). The GSM_ST value of drainage_agreed with the green shading decreases with the decrease of the scale. In comparison with the drainage networks at the original scale (1:24,000), the greater the differences in drainage morphology, the lower the GSM_ST value for drainage_agreed. The drainage_agreed at 1:50,000 in cases 1, 17, 54, and 59 maintain the consistency of their global spatial form and drainage density distribution, resulting in a GSM_ST value greater than 0.7. At 1:100,000, the drainage_agreed retains its global spatial morphological consistency but with a significantly different drainage density, resulting in a GSM_ST value lower than at 1:50,000 but still larger than 0.5. At 1:250,000, the drainage_agreed map indicates a significant generalization of the drainage network morphology. While maintaining the primary streams and overall extension direction of the original drainage network, there exist notable dissimilarities in spatial morphology and drainage density, leading to a marked reduction in GSM_ST value (less than 0.5) compared to previous scales. For drainage_agreed at 1:500,000 and 1:1,000,000 scales, there is a significant reduction in the number of rivers, with only the most crucial streams retained. This results in low GSM_ST values (less than 0.4 and less than 0.3, respectively). Conversely, when analyzing the visualization of drainage_disagreed for cases 3, 16, and 38, the GSM_ST values exhibit high consistency in spatial morphological cognition at 1:50,000 and 1:100,000 scales. However, at scales of 1:250,000, 1:500,000, and 1:000,000, the GSM_ST values contradict spatial cognition. For example, in case 3, the 1:500,000 drainage_disagreed intensively generalizes the fan shape of the drainage_original, while the 1:1,000,000

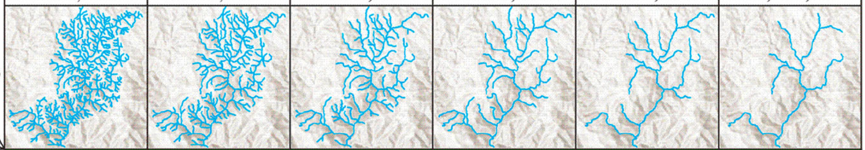

Case 43 / GSM_ST / Method	1:24,000	1:50,000	1:100,000	1:250,000	1:500,000	1:1,000,000
DNC_GAE	1.00	0.7832	0.5991	0.3764	0.3246	0.2620
FSD_GAE	1.00	0.7298	0.5404	0.3980	0.3321	0.3112
CE_GAE	1.00	0.9337	0.8709	0.7644	0.6756	0.5466
SIM_global	1.00	0.8518	0.7942	0.7059	0.6322	0.5350

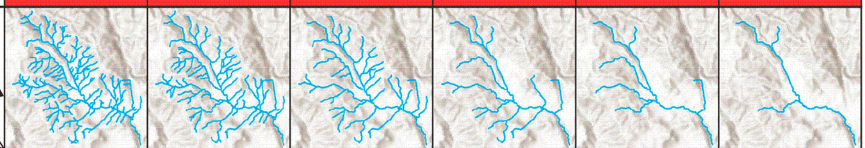

Case 57 / GSM_ST / Method	1:24,000	1:50,000	1:100,000	1:250,000	1:500,000	1:1,000,000
DNC_GAE	1.00	0.8197	0.6697	0.5608	0.3691	0.2648
FSD_GAE	1.00	0.6698	0.5886	0.3550	0.3547	0.2886
CE_GAE	1.00	0.9173	0.8466	0.7484	0.6105	0.5495
SIM_global	1.00	0.8936	0.8013	0.7028	0.6328	0.4814

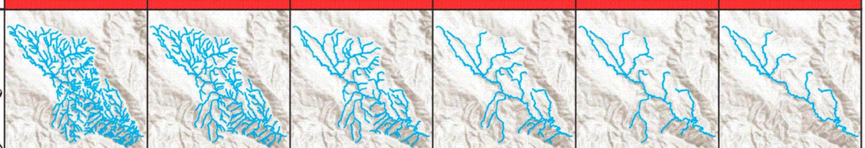

Case 60 / GSM_ST / Method	1:24,000	1:50,000	1:100,000	1:250,000	1:500,000	1:1,000,000
DNC_GAE	1.00	0.7579	0.6169	0.4725	0.3147	0.2466
FSD_GAE	1.00	0.4916	0.3433	0.2782	0.1644	0.0451
CE_GAE	1.00	0.9076	0.8595	0.7409	0.5817	0.5119
SIM_global	1.00	0.8710	0.7881	0.6901	0.6376	0.6055

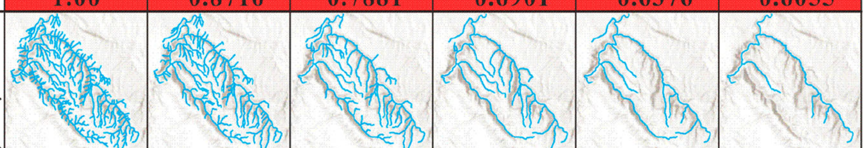

Case 64 / GSM_ST / Method	1:24,000	1:50,000	1:100,000	1:250,000	1:500,000	1:1,000,000
DNC_GAE	1.00	0.7884	0.6231	0.4695	0.3131	0.2232
FSD_GAE	1.00	0.6348	0.3688	0.2135	0.1496	0.1621
CE_GAE	1.00	0.9150	0.8454	0.7104	0.6625	0.3778
SIM_global	1.00	0.8941	0.8230	0.7226	0.6634	0.5841

Figure 17. Visualization of typical cases from the questionnaire survey on GSM_ST implemented by DNC_GAE, FSD_GAE, CE_GAE, and SIM_global. The background color of each case represents the level of agreement among the respondents: a green background indicates that more than half of the respondents agreed with the scheme, while a red background indicates that the scheme did not receive the approval of more than half of the respondents. Source of hillshade: http://goto.arcgisonline.com/maps/Elevation/World_Hillshade. (DNC_GAE is our proposed method; FSD_GAE is the GAE using Fourier shape descriptor; CE_GAE is the GAE using coordinate embedding; SIM_global is a typical traditional method.)

drainage_disagreed deviates seriously from the original fan shape. Strangely the latter exhibits a slightly higher GSM_ST value than the former. This situation also occurs in case 16 at the scales of 1:250,000 and 1:500,000, and in case 38 at the scales of 1:500,000 and 1:1,000,000. Besides, in cases 16 and 38 at the 1:1,000,000 scale, the GSM_ST values are excessively high (0.4185 and 0.4009, respectively), whereas values below 0.3 would be more reasonable given their spatial morphology.

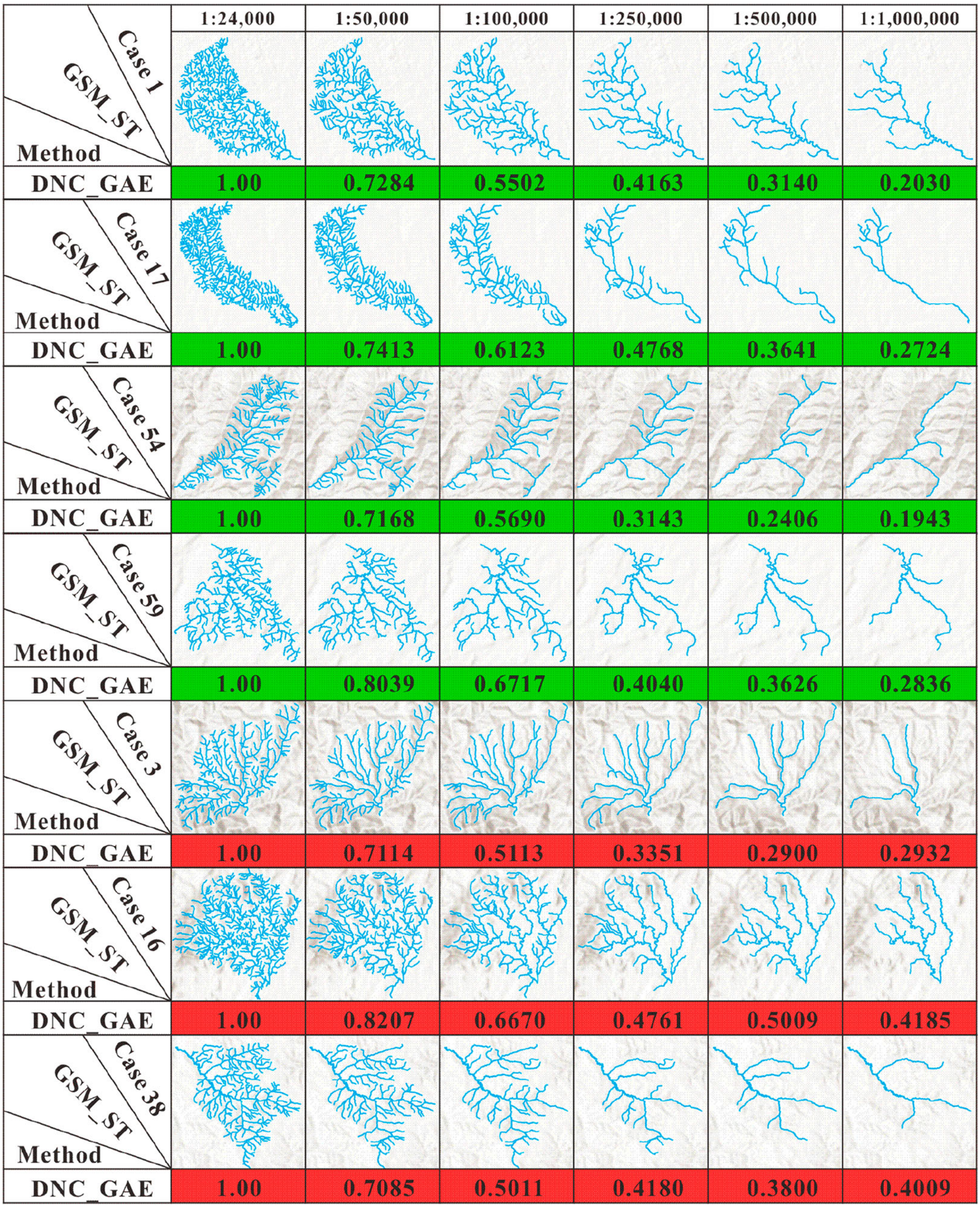

Figure 18. Visualization of the questionnaire survey on the GSM_ST scheme implemented by DNC_GAE (case number is consistent with Figure 16 (a)). Source of hillshade: http://goto.arcgisonline.com/maps/Elevation/World_Hillshade. (DNC_GAE is our proposed method; FSD_GAE is the GAE using Fourier shape descriptor; CE_GAE is the GAE using coordinate embedding; SIM_global is a typical traditional method.)

The visualization analysis of the GSM_ST results in Figure 18 reveals that the opinions of the interviewee align with the performance of the DNC_GAE: the GSM_ST schemes that appear reasonable receive the agreement, while the unreasonable ones do not. This finding further substantiates the reliability of the 87.69% satisfaction ratio for the DNC_GAE.

4.5.2. Comparison discussion

In this section, we discuss the performance of both the DNC_GAE and SIM_global (Yan, Shen, and Li 2016; Yang and Wang 2021), a traditional similarity measurement method, in GSM_ST. Based on the results presented in Figure 16, the DNC_GAE outperforms SIM_global. While the GSM_ST scheme using SIM_global exhibits a decreasing trend as the drainage network morphology simplifies (see Figure 17), it is worth noting that the GSM_ST values at small scales are excessively high and fail to reflect the intensively generalized morphology of the drainage network accurately. For example, its GSM_ST value at a scale of 1:500,000 (ranging between 0.6-0.7) exceeds the normal range of 0.3-0.4, while at a scale of 1:1,000,000 (ranging between 0.4-0.6), the GSM_ST value is beyond the normal range of 0.2-0.3. As demonstrated in Table 2, only five cases were agreed upon by the respondents, resulting in a low satisfaction ratio of 7.69%, which is significantly below the satisfaction ratio of DNC_GAE of 87.69%. Furthermore, Table 3 illustrates that DNC_GAE was chosen as the optimal method in 51 cases, while SIM_global was only selected in one case. These findings highlight the superior robustness of DNC_GAE compared to SIM_global in the context of GSM_ST.

The geometric similarity of drainage networks is the degree of coincidence of the spatial cognition of the drainage network morphology before and after scaling transformation, a whole, unreadable, and abstract mapping from the brain. This process involves the perception of geometric morphological features, Gestalt psychology, and other human cognition principles such as similarity, continuity, and proximity (Wertheimer and Riezler 1944; Ai et al. 2015; Yan, Shen, and Li 2016). Due to the abstract of this process, it is challenging to quantify the spatial cognition information of the drainage network morphology using specific characteristics.

Although both DNC_GAE and SIM_global are designed to achieve GSM_ST by mining multi-dimensional information about drainage morphology before and after scaling transformation, there are significant differences in their mining mechanism and level of spatial cognition information of the drainage network morphology. SIM_global uses easily understandable features based on known spatial relationships, including topological similarity, directional similarity, distance similarity, and geometric features, to represent drainage morphological cognition. On the other hand, DNC_GAE acquires a deep and abstract representation of the cognition of drainage morphology through graph convolution that leverages these features. This enables DNC_GAE to compute a more abstract and informative embedding by aggregating information from adjacent nodes, which is more similar to how the brain processes information. Thus, the drainage network embedding obtained through GAE has more complete and accurate information about the spatial cognition of the drainage network morphology, making the GSM_ST based on the DNC_GAE more objective and robust.

5. Conclusions

This study proposes an unsupervised-learning GAE model, called DNC_GAE, that integrates drainage network characteristics to tackle the complex uncertainty problem of geometric similarity measurement in scaling transformation (GSM_ST) involving spatial cognition. The experimental results show that the DNC_GAE method achieves an excellent fit with the optimal hyperparameters combination obtained from the sensitivity analysis. To evaluate the effectiveness of DNC_GAE, a questionnaire survey was conducted with 23 cartography professionals and students, testing GSM_ST results of 71 drainage cases using various methods. Statistical analysis shows that GSM_ST results implemented by DNC_GAE are consistent with the gradual simplification of the drainage network morphology during scaling transformation with a reasonable scheme. Additionally, the proposed DNC_GAE outperforms other methods, including the alternative unsupervised representation learning methods, the GAE supported by different features, and the state-of-the-art method, with a satisfaction rate of around 88%. Therefore, the GAE integrating drainage network characteristics is an objective and robust method for conducting GSM_ST.

This study still has two deficiencies. Firstly, the semantic information of drainage networks was not considered, and future research should include semantic information such as river name, classification, and seasonality as node features in the drainage graph through one-hot encoding. When scaling a drainage network from a large scale to a small scale, it is important to retain both its geometric and semantic information with limited rivers, whereas this study only focused on the geometric aspect of similarity. Secondly, DNC_GAE does not facilitate the information exchange between the drainage graphs before and after scaling transformation, which impeded the end-to-end similarity measurement. Instead, the Cosines similarity was used to calculate the distance between the drainage embeddings, which only accounts for the difference in the drainage network morphology at the whole graph level, neglecting the information interaction between nodes. To overcome this, graph neural networks like SimGNN (Bai et al. 2019) can be introduced to conduct the feature interaction between the graph and node levels, followed by a fully connected network to calculate the similarity value.

Acknowledgements

We appreciate the detailed suggestions and comments from editors and anonymous reviewers. We express heartfelt thanks to all questionnaire survey participants. Weiming Huang acknowledges the financial support from the Knut and Alice Wallenberg Foundation, and Lars Harrie acknowledges the financial support from Lund University.

Disclosure statement

No potential conflict of interest was reported by the author(s).

Funding

This work was supported by the National Natural Science Foundation of China [grant number 41531180], the National Natural Science Foundation of China [grant number 42071450], and the China Scholarship Council (CSC) [grant number 202206270076]. Weiming Huang acknowledges the financial support from the Knut and Alice Wallenberg Foundation.

Data availability statement

The study data and codes that support the findings of this study are available at a link: https://figshare.com/s/81bfdf296638c29c3894.

ORCID

Huafei Yu http://orcid.org/0000-0002-2542-5246
Tinghua Ai http://orcid.org/0000-0002-6581-9872
Min Yang http://orcid.org/0000-0003-1973-527X
Weiming Huang http://orcid.org/0000-0002-3208-4208
Lars Harrie http://orcid.org/0000-0003-3252-1495

References

Ai, T. 2007. "The Drainage Network Extraction from Contour Lines for Contour Line Generalization." *ISPRS Journal of Photogrammetry and Remote Sensing* 62 (2): 93–103. doi:10.1016/j.isprsjprs.2007.04.002.

Ai, T., S. Ke, M. Yang, and J. Li. 2017. "Envelope Generation and Simplification of Polylines Using Delaunay Triangulation." *International Journal of Geographical Information Science* 31 (2): 297–319. doi:10.1080/13658816.2016.1197399.

Ai, T., M. Yang, X. Zhang, and J. Tian. 2015. "Detection and Correction of Inconsistencies between River Networks and Contour Data by Spatial Constraint Knowledge." *Cartography and Geographic Information Science* 42 (1): 79–93. doi:10.1080/15230406.2014.956673.

Ai, T., Q. Zhou, X. Zhang, Y. Huang, and M. Zhou. 2014. "A Simplification of ria Coastline with Geomorphologic Characteristics Preserved." *Marine Geodesy* 37 (2): 167–186. doi:10.1080/01490419.2014.903215.

Argialas, D., J. Lyon, and O. Mintzer. 1988. "Quantitative Description and Classification of Drainage Patterns." *Photogrammetric Engineering and Remote Sensing* 54 (4): 505–509. http://www.scopus.com/inward/record.url?eid=2-s2.0-0024165267&partnerID=MN8TOARS.

Atwood, J., and D. Towsley. 2016. "Diffusion-Convolutional Neural Networks." In *Advances in neural information processing systems*.

Bai, Y., H. Ding, S. Bian, T. Chen, Y. Sun, and W. Wang. 2019. "Simgnn: A Neural Network Approach to Fast Graph Similarity Computation." Proceeding of the Twelfth ACM International Conference on Web Search and Data Mining: 384–92. doi:10.1145/3289600.3290967.

Bai, Y., H. Ding, Y. Sun, and W. Wang. 2018. "Convolutional Set Matching for Graph Similarity." *arXiv preprint arXiv:1810.10866*. doi:10.48550/arXiv.1810.10866.

Bajracharya, P., and S. Jain. 2022. "Hydrologic Similarity Based on Width Function and Hypsometry: An Unsupervised Learning Approach." *Computers & Geosciences* 163: 105097. doi:10.1016/j.cageo.2022.105097.

Bouramtane, T., A. Tiouiouine, I. Kacimi, V. Valles, A. Talih, N. Kassou, J. Ouardi, et al. 2020. "Drainage Network Patterns Determinism: A Comparison in Arid, Semi-Arid and Semi-Humid Area of Morocco Using Multifactorial Approach." *Hydrology* 7 (4): 87. doi:10.3390/hydrology7040087.

Davis, L. S. 1991. "Shape Representation and Matching." In *Pattern Recognition and Image Processing in Physics*, edited by R. A. Vaughan, 101–128. Bristol, England: Adam Hilger.

Duvenaud, D., D. Maclaurin, J. Iparraguirre, R. Bombarell, T. Hirzel, A. Aspuru-Guzik, and R. P. Adams. 2015. "Convolutional networks on graphs for learning molecular fingerprints." In *Advances in neural information processing systems*.

Fahrul, H., P. Nugroho, S. D. Budi, H. M. Irwan, R. Tia, R. Nuzula, and W. Rizka. 2020. "Stream order selection for model generalization of the topographic map of Indonesia." In *IOP Conference Series: Earth and Environmental Science*, 012022. IOP Publishing.

Gao, J., and X. Cao. 2021. "The new Development Direction of Cartorgraphy Promoted by Spatial Cognition." *Acta Geodaetica et Cartographica Sinica* 50 (6): 711–725. doi:10.11947/j.AGCS.2021.20210043.

Howard, A. D. 1967. "Drainage Analysis in Geologic Interpretation: A Summation." *AAPG Bulletin* 51 (11): 2246–2259. doi:10.1306/5D25C26D-16C1-11D7-8645000102C1865D.

Kimberling, A. J., A. R. Buckley, P. C. Muehrcke, and J. O. Muehrcke. 2012. *Map use: Reading, Analysis, Interpretation*. Redlands, USA: ESRI Press Academic.

Kipf, T. N., and M. Welling. 2016. "Variational Graph Auto-Encoders." *arXiv preprint arXiv:1611.07308*. doi:10.48550/arXiv.1611.07308.

Kipf, T. N., and M. Welling. 2017. "Semi-Supervised Classification with Graph Convolutional Networks." In *the 5th International Conference on Learning Representations*. Toulon, France.

Li, Y., C. Gu, T. Dullien, O. Vinyals, and P. Kohli. 2019. "Graph Matching Networks for Learning the Similarity of Graph Structured Objects." In *International conference on machine learning*, 3835-45. PMLR.

Li, P., H. Yan, and X. Lu. 2022. "A Siamese Neural Network for Learning the Similarity Metrics of Linear Features." *International Journal of Geographical Information Science*, 1–28. doi:10.1080/13658816.2022.2143505.

Liao, L., X. He, H. Zhang, and T.-S. Chua. 2018. "Attributed Social Network Embedding." *IEEE Transactions on Knowledge and Data Engineering* 30 (12): 2257–2270. doi:10.1109/TKDE.2018.2819980.

Liu, P., X. Huang, H. Ma, and M. Yang. 2022. "Fourier Descriptor-Based Neural Network Method for High-Precision Shape Recognition of Building Polygon." *Acta Geodaetica et Cartographica Sinica* 51 (9): 1969–1976. doi:10.11947/j.AGCS.2022.20210730.

Liu, J., G. Ma, F. Jiang, C.-T. Lu, S. Y. Philip, and A. B. Ragin. 2019. "Community-Preserving Graph Convolutions for Structural and Functional Joint Embedding of Brain Networks." In 2019 *IEEE International Conference on Big Data (Big Data)*, 1163-8. IEEE.

Liu, P., T. Xiao, J. Xiao, and T. Ai. 2020. "A Multi-Scale Representation Model of Polyline Based on Head/Tail Breaks." *International Journal of Geographical Information Science* 34 (11): 2275–2295. doi:10.1080/13658816.2020.1753203.

Ma, G., N. K. Ahmed, T. L. Willke, D. Sengupta, M. W. Cole, N. B. Turk-Browne, and P. S. Yu. 2019. "Deep Graph Similarity Learning for Brain Data Analysis." Proceeding of the 28th ACM International Conference on Information and Knowledge Management: 2743-51. doi:10.1145/3357384.3357815.

Ma, G., C.-T. Lu, L. He, S. Y. Philip, and A. B. Ragin. 2017. "Multi-View Graph Embedding with Hub Detection for Brain Network Analysis." In 2017 *IEEE International Conference on Data Mining (ICDM)*, 967-72. IEEE.

Mazur, R. E., and H. W. Castner. 1990. "Horton's Ordering Scheme and the Generalisation of River Networks." *The Cartographic Journal* 27 (2): 104–112. doi:10.1179/000870490787858775.

Mejia, A. I., and J. D. Niemann. 2008. "Identification and Characterization of Dendritic, Parallel, Pinnate, Rectangular, and Trellis Networks Based on Deviations from Planform Self-Similarity." *Journal of Geophysical Research-Earth Surface* 113 (F2): F02015. doi:10.1029/2007JF000781.

Roberts, G. G. 2019. "Scales of Similarity and Disparity Between Drainage Networks." *Geophysical Research Letters* 46 (7): 3781–3790. doi:10.1029/2019GL082446.
Rozemberczki, B., C. Allen, and R. Sarkar. 2021. "Multi-scale Attributed Node Embedding." *Journal of Complex Networks* 9 (2): cnab014. doi:10.1093/comnet/cnab014.
Shreve, R. L. 1966. "Statistical Law of Stream Numbers." *The Journal of Geology* 74 (1): 17–37. doi:10.1086/627137.
Stanislawski, L. V. 2009. "Feature Pruning by Upstream Drainage Area to Support Automated Generalization of the United States National Hydrography Dataset." *Computers Environment and Urban Systems* 33 (5): 325–333. doi:10.1016/j.compenvurbsys.2009.07.004.
Stanislawski, L. V., B. P. Buttenfield, and A. Doumbouya. 2015. "A Rapid Approach for Automated Comparison of Independently Derived Stream Networks." *Cartography and Geographic Information Science* 42 (5): 435–448. doi:10.1080/15230406.2015.1060869.
Stanislawski, L. V., B. P. Buttenfield, M. P. Finn, and K. Roth. 2009. "Stratified Database Pruning to Support Local Density Variations in Automated Generalization of the United States National Hydrography Dataset." In *the 24 th International Cartographic Conference (ICC2009)*. Santiago, Chile.
Strahler, A. N. 1957. "Quantitative Analysis of Watershed Geomorphology." *Transactions of the American Geophysical Union* 38 (6): 913–920. doi:10.1029/TR038i006p00913.
Thomson, R. C., and R. Brooks. 2002. "Exploiting Perceptual Grouping for Map Analysis, Understanding and Generalization: The Case of Road and River Networks." In *International Workshop on Graphics Recognition*, edited by D. Blostein, and Y.-B. Kwon, 148–157. Berlin, Heidelberg: Springer.
Töpfer, F., and W. Pillewizer. 1966. "The Principles of Selection." *The Cartographic Journal* 3 (1): 10–16. doi:10.1179/caj.1966.3.1.10.
Tversky, A. 1977. "Features of Similarity." *Psychological Review* 84 (4): 327. doi:10.1037/0033-295X.84.4.327
Veličković, P., W. Fedus, W. L. Hamilton, P. Liò, Y. Bengio, and R. D. Hjelm. 2018. "Deep Graph Infomax." *arXiv preprint arXiv:1809.10341*. doi:10.48550/arXiv.1809.10341.
Wertheimer, M., and K. Riezler. 1944. "Gestalt Theory." *Social Research* 11: 78–99.
Xia, F., K. Sun, S. Yu, A. Aziz, L. Wan, S. Pan, and H. Liu. 2021. "Graph Learning: A Survey." *IEEE Transactions on Artificial Intelligence* 2 (2): 109–127. doi:10.1109/TAI.2021.3076021.
Yan, H. 2019. "Description and Generalization of River Networks." In *Description Approaches and Automated Generalization Algorithms for Groups of Map Objects*, edited by H. Yan, 109–148. Singapore: Springer.
Yan, H. 2022. "Quantifying Spatial Similarity for use as Constraints in Map Generalisation." *Journal of Spatial Science*, 1–20. doi:10.1080/14498596.2022.2154713.
Yan, X. F., T. H. Ai, M. Yang, and X. H. Tong. 2021. "Graph Convolutional Autoencoder Model for the Shape Coding and Cognition of Buildings in Maps." *International Journal of Geographical Information Science* 35 (3): 490–512. doi:10.1080/13658816.2020.1768260.
Yan, H., and J. Li. 2015. *Spatial Similarity Relations in Multi-Scale map Spaces*. Cham: Springer.
Yan, H., Y. Shen, and J. Li. 2016. "Approach to Calculating Spatial Similarity Degrees of the Same River Basin Networks on Multi-Scale Maps." *Geocarto International* 31 (7): 765–782. doi:10.1080/10106049.2015.1076063.
Yang, F., and Z. Wang. 2021. "River Systems Geometric Similarity Measurement Method Under Hierarchical Analysis." *Journal of Geo-Information Science* 23 (12): 2139–2150. doi:10.12082/dqxxkx.2021.210279.
Ying, Z., J. You, C. Morris, X. Ren, W. Hamilton, and J. Leskovec. 2018. "Hierarchical Graph Representation Learning with Differentiable Pooling." In *Advances in neural information processing systems.*
Yu, H., T. Ai, M. Yang, L. Huang, and J. Yuan. 2022. "A Recognition Method for Drainage Patterns Using a Graph Convolutional Network." *International Journal of Applied Earth Observation and Geoinformation* 107: 102696. doi:10.1016/j.jag.2022.102696.
Yu, W., and Q. Huang. 2022. "A Deep Encoder-Decoder Network for Anomaly Detection in Driving Trajectory Behavior Under Spatio-Temporal Context." *International Journal of Applied Earth Observation and Geoinformation* 115: 103115. doi:10.1016/j.jag.2022.103115.
Zhang, Z., J. Bu, M. Ester, J. Zhang, C. Yao, Z. Yu, and C. Wang. 2019. "Hierarchical Graph Pooling with Structure Learning." *arXiv preprint arXiv:1911.05954*. doi:10.48550/arXiv.1911.05954.
Zhang, L., and E. Guilbert. 2012. "A Study of Variables Characterizing Drainage Patterns in River Networks." *International Archives of the Photogrammetry, Remote Sensing and Spatial Information Sciences* 39 (B2): 29–34. doi:10.5194/isprsarchives-XXXIX-B2-29-2012.
Zhang, L., and E. Guilbert. 2016. "Evaluation of River Network Generalization Methods for Preserving the Drainage Pattern." *ISPRS International Journal of Geo-Information* 5 (12). doi:10.3390/ijgi5120230.
Zhang, L., and E. Guilbert. 2017. "A Genetic Algorithm for Tributary Selection with Consideration of Multiple Factors." *Transactions in Gis* 21 (2): 332–358. doi:10.1111/tgis.12205.
Zhang, Y., and W. Yu. 2022. "Detecting Common Features from Point Patterns for Similarity Measurement Using Matrix Decomposition." *Cartography and Geographic Information Science*, 1–24. doi:10.1080/15230406.2022.2125078.
Zhao, R., T. H. Ai, W. H. Yu, Y. K. He, and Y. L. Shen. 2020. "Recognition of Building Group Patterns Using Graph Convolutional Network." *Cartography and Geographic Information Science* 47 (5): 400–417. doi:10.1080/15230406.2020.1757512.